Last time | Glauber - Gribov - Mueller Multiple-Rescatterings Formula (cont'd)

We considered scattering of a dipole on many nucleons in the nucleus: we showed that the scattering processes on individual nucleons happen separate from each other.

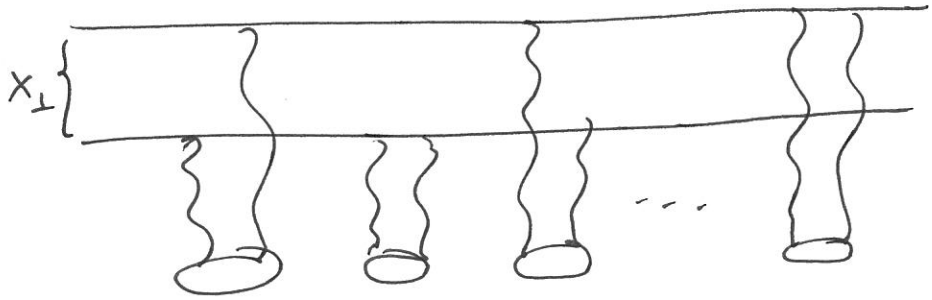

We arrived at the following expression for N:

$$N(\underline{x},\underline{b}) = 1 - \exp\left\{-\frac{\alpha_s^2 C_F \bar{n}}{N_c}\, T(\underline{b})\, x_\perp^2 \ln\frac{1}{x_\perp \Lambda}\right\}$$

where each nucleon is modeled by a single quark with the IR cutoff Λ.

$$T(\underline{b}) \equiv \int_{-\infty}^{\infty} db_3\, \rho(\underline{b}, b_3)$$

$\leftarrow$ nuclear profile fn.

ρ = nucleon # density.

Going back to the nuclear rest frame and remembering that $S(\vec{x}_\perp) = s(\vec{x}_\perp, L)$, we obtain

$$S(\vec{x}_\perp, \vec{b}_\perp, Y = 0) = \exp\left\{-\frac{\sigma^{q\bar{q}N}}{2} T(\vec{b}_\perp)\right\}. \tag{4.44}$$

Note that $\sigma^{q\bar{q}N}$ does not depend on the energy of the collision (and therefore on its net rapidity): to underscore this we have put $Y = 0$ in the argument of the S-matrix in Eq. (4.44). This will delineate this expression from the energy-dependent version that results from incorporating small-x evolution into this picture.

Using Eq. (4.44) along with Eq. (4.28) in Eq. (4.38), the imaginary part of the forward scattering amplitude in the Glauber–Gribov–Mueller (GGM) model (Mueller 1990) is given by

$$N(\vec{x}_\perp, \vec{b}_\perp, Y = 0) = 1 - \exp\left\{-\frac{\alpha_s \pi^2}{2N_c} T(\vec{b}_\perp) x_\perp^2 x G_N\left(x, \frac{1}{x_\perp^2}\right)\right\}. \tag{4.45}$$

This is the GGM multiple–rescattering formula. Note again that the nucleon's gluon distribution function xG_N in Eq. (4.45) is taken at the lowest, two-gluon, level and is thus independent of x, so that the amplitude N in Eq. (4.45) is independent of energy.

Equation (4.45) has a remarkable property: one can see that it implies $N \leq 1$ for all (perturbative) $x_\perp$. This means that the resulting forward scattering amplitude obeys the black-disk limit constraint (4.33), correcting the problem of the single rescattering amplitude from Eq. (4.32). We see that multiple rescatterings unitarize the scattering cross section, preserving the black-disk limit. The lesson we learn from the Glauber–Gribov–Mueller model is that to unitarize a cross section it is important to include multiple rescatterings!

Equation (4.45) allows us to determine the parameter corresponding to resummation of the diagrams like that shown in Fig. 4.5. Using the gluon distribution from Eq. (4.27) in Eq. (4.45), and noting that for large nuclei the profile function $T(\vec{b}_\perp)$ scales as $A^{1/3}$, we conclude that the resummation parameter of multiple rescatterings is (Kovchegov 1997)

$$\alpha_s^2 A^{1/3}. \tag{4.46}$$

The physical meaning of the parameter $\alpha_s^2 A^{1/3}$ is rather straightforward: at a given impact parameter the dipole interacts with $\sim A^{1/3}$ nucleons, exchanging two gluons with each. Since two-gluon exchange is parametrically of order α_s^2 we obtain $\alpha_s^2 A^{1/3}$ as the resummation parameter.

4.2.3 Saturation picture from the GGM formula

Multiple nucleon interactions become important in Eq. (4.45) when the dipole size becomes of order $x_\perp \sim 1/Q_s$, where the *saturation* scale Q_s is defined by the following implicit equation (cf. Eq. (3.133)):

$$Q_s^2(\vec{b}_\perp) = \frac{\alpha_s \pi^2}{2N_c} T(\vec{b}_\perp) x G_N(x, Q_s^2). \tag{4.47}$$

Note that for a cylindrical nucleus, as considered in Sec. 3.4.2, one has $T(\vec{b}_\perp) = A/S_\perp$ so that, taking into account that the nuclear gluon distribution is $xG_A = AxG_N$ (which is

P1: SFK Trim: 247mm × 174mm Top: 13.707mm Gutter: 18.98mm
CUUK1947-04 CUUK1947/Kovchegov 978 0 521 11257 4 March 23, 2012 20:28

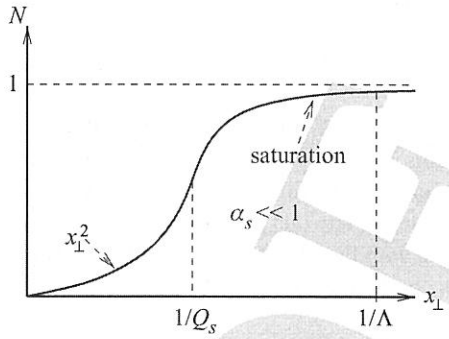

Fig. 4.11. The imaginary part of the forward amplitude of the dipole–nucleus scattering N plotted as a function of the transverse separation between the quark and the anti-quark in a dipole $x_\perp$, using Eq. (4.51). (Reprinted from Jalilian-Marian and Kovchegov (2006), with permission from Elsevier.) A color version of this figure is available online at www.cambridge.org/9780521112574.

true at the two-gluon level considered here), one can recast Eq. (4.47) in almost the exact form of Eq. (3.133). The difference N_c/C_F between the saturation scales in (4.47) and in (3.133) is due to the fact that the saturation scale (4.47) we have just found is that for a quark dipole, whereas the saturation scale in Eq. (3.133) was obtained solely for gluons. If we were to replace the quark dipole in Fig. 4.5 with a gluon dipole, we would need to modify the exponent in Eq. (4.45) by the ratio of the adjoint and fundamental Casimir operators N_c/C_F, putting Eq. (4.47) in exact agreement with Eq. (3.133). With this proviso, we see that, at least at the lowest order considered, Eq. (4.47) gives the same saturation scale as what follows from the GLR–MQ equation.

Inserting the lowest-order single-quark gluon distribution function,

$$xG_{LO}^{quark}(x, Q_\perp^2) = \frac{\alpha_s C_F}{\pi} \ln \frac{Q^2}{\Lambda^2}, \tag{4.48}$$

into Eq. (4.45), we can rewrite it as

$$N(\vec{x}_\perp, \vec{b}_\perp, Y = 0) = 1 - \exp\left\{-\frac{\alpha_s^2 C_F \pi}{N_c} T(\vec{b}_\perp) x_\perp^2 \ln \frac{1}{x_\perp \Lambda}\right\}. \tag{4.49}$$

Defining the quark *saturation* scale (note the factor 4 difference compared with Eq. (4.47) and the absence of a gluon distribution in this definition),

$$Q_s^2(\vec{b}_\perp) \equiv \frac{4\pi \alpha_s^2 C_F}{N_c} T(\vec{b}_\perp), \tag{4.50}$$

we rewrite Eq. (4.49) as

$$N(\vec{x}_\perp, \vec{b}_\perp, Y = 0) = 1 - \exp\left\{-\frac{x_\perp^2 Q_s^2(\vec{b}_\perp)}{4} \ln \frac{1}{x_\perp \Lambda}\right\}. \tag{4.51}$$

The dipole amplitude N from Eq. (4.51) is plotted schematically in Fig. 4.11 as a function of $x_\perp$. One can see that, at small $x_\perp$, i.e., $x_\perp \ll 1/Q_s$, we have $N \sim x_\perp^2$ so that the amplitude

is zero for zero dipole size. This result is natural, since in a zero-size dipole the color charges of the quark and the antiquark cancel each other, leading to the disappearance of interactions with the target. This effect is known as *color transparency* (Kopeliovich, Lapidus, and Zamolodchikov 1981, Nikolaev and Zakharov 1991, Heiselberg *et al.* 1991, Blaettel *et al.* 1993, Frankfurt, Miller, and Strikman 1993).

The amplitude (4.51) is a rising function of $x_\perp$ at small dipole size. However, at large dipole size $x_\perp \gtrsim 1/Q_s$, growth stops and the amplitude levels off (*saturates*) at $N = 1$. As mentioned earlier, this regime corresponds to the black-disk limit for dipole–nucleus scattering: for large dipoles the nucleus appears as a black disk. The transition from $N \sim x_\perp^2$ to the black disk-like ($N = 1$) behavior in Fig. 4.11 occurs at around $x_\perp \sim 1/Q_s$. For dipole sizes $x_\perp \gtrsim 1/Q_s$ the amplitude N *saturates* to a constant. This translates into saturation of the quark distribution functions in the nucleus, since $xq + x\bar{q} \sim F_2$ (see Eq. (2.46)) and the saturation of N implies the saturation of F_2, as follows from Eqs. (4.10a), (4.12), and (4.24). Thus the saturation of N can be identified with parton saturation, justifying the name *saturation scale* for Q_s, Eq. (4.50).

Note that since $T(\vec{b}_\perp) \sim A^{1/3}$ the saturation scale grows as

$$Q_s^2 \sim A^{1/3} \tag{4.52}$$

with atomic number A. If A is large enough, Q_s becomes perturbatively large, $Q_s \gg \Lambda_{QCD}$, justifying the use of perturbation theory. The scaling in Eq. (4.52) is consistent with Eq. (3.135), which we obtained from analyzing the GLR equation.

4.3 Mueller's dipole model and Nonlinear Small-x Evolution

The amplitude N given by the Glauber–Gribov–Mueller formula (4.51) is independent of the energy of the collision (see also Eq. (4.49)) and therefore cannot be the final answer for the high energy scattering problem at hand. It turns out that the energy dependence comes into the dipole–nucleus scattering amplitude through quantum evolution corrections, much as the two-gluon exchange amplitude in the onium–onium scattering in Sec. 3.2 acquires energy dependence through the BFKL evolution of Sec. 3.3. To incorporate small-x evolution into dipole–nucleus scattering we begin by rewriting the evolution in the language of LCPT, in which it can be completely absorbed into the light cone wave function, with the help of Mueller's dipole model (Mueller 1994, 1995, Mueller and Patel 1994).

4.3.1 Dipole wave function and generating functional

Let us consider the light cone wave function of an ultrarelativistic meson consisting of a heavy quark and antiquark (an onium), with no sea quarks and gluons present before the small-x evolution, as shown in Fig. 4.12. We can safely apply perturbative QCD to the onium wave function since here typical transverse distance $x_\perp$ is about $1/m_Q$, where m_Q is the large mass of the heavy quark; the strong coupling constant is clearly small at such distances.

We will denote the "bare" onium light cone wave function by $\Psi^{(0)}_{\sigma\sigma'}(\vec{k}_\perp, z)$ (cf. Eq. (4.19)), where $\vec{k}_\perp$ is the relative transverse momentum of the $q\bar{q}$ pair, $z = k^+/p^+$ is the fraction of the light cone momentum p^+ of the whole onium carried by the quark, while σ and σ' are

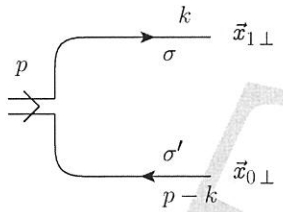

Fig. 4.12. The onium light cone wave function before small-x evolution.

the polarizations of the quark and the antiquark (see Fig. 4.12). The onium is moving in the light cone plus direction. As usual we suppress the color and flavor indices, assuming that they will be properly summed over when necessary. As we will shortly see, the transverse size of the dipole remains invariant during the small-x evolution: therefore we will work in a mixed representation where we use the transverse coordinates and longitudinal momenta to describe dipoles. We thus Fourier-transform the onium wave function, using

$$\Psi^{(0)}_{\sigma\sigma'}(\vec{x}_{10}, z) = \int \frac{d^2k_\perp}{(2\pi)^2} e^{i\vec{k}_\perp \cdot \vec{x}_{10}} \Psi^{(0)}_{\sigma\sigma'}(\vec{k}_\perp, z), \tag{4.53}$$

where $\vec{x}_{10\perp} = \vec{x}_{1\perp} - \vec{x}_{0\perp}$ is the transverse size of dipole, the quark being located at $\vec{x}_{1\perp}$ and the antiquark at $\vec{x}_{0\perp}$ (see Fig. 4.12).

As the initial onium state contains only the $q\bar{q}$ pair its normalization is (cf. Eqs. (1.70) and (1.82))

$$\int_0^1 \frac{dz}{z(1-z)} \int \frac{d^2k_\perp}{2(2\pi)^3} \sum_{\sigma,\sigma'} \left| \Psi^{(0)}_{\sigma\sigma'}(\vec{k}_\perp, z) \right|^2 = 1, \tag{4.54}$$

which, in transverse coordinate space becomes

$$\int_0^1 \frac{dz}{z(1-z)} \int \frac{d^2x_{10}}{4\pi} \sum_{\sigma,\sigma'} \left| \Psi^{(0)}_{\sigma\sigma'}(\vec{x}_{10}, z) \right|^2 = 1. \tag{4.55}$$

We are interested in modifications to this wave function under small-x evolution in the LLA approximation; thus we need to resum the terms containing $\alpha_s \ln 1/x$ corrections. Throughout this section we will work in the $A^+ = 0$ light cone gauge. As for the DGLAP evolution of Sec. 2.4.2, one step of LLA small-x evolution consists of the appearance of a single gluon in the wave function: the gluon can be emitted either from the quark line or from the antiquark line, as shown in Fig. 4.13. (Just as in the case of BFKL evolution, quark loops and the emission of $q\bar{q}$ pairs are beyond the LLA, contributing subleading corrections of order $\alpha_s^2 \ln 1/x$.) The corresponding modification of the onium wave function due to the gluon emissions in Fig. 4.13 is easier to calculate than in the DGLAP case. We assume that the light cone momentum k_2^+ of the emitted gluon is small, $k_2^+ \ll k_1^+, p^+ - k_1^+$ (see

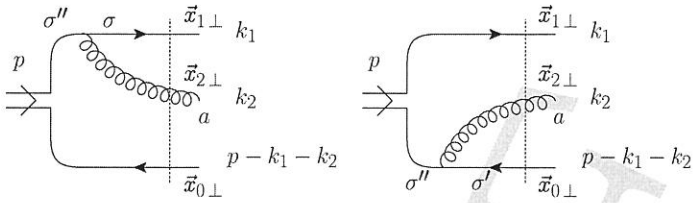

Fig. 4.13. One step of small-x evolution in the onium wave function. The dotted lines denote the intermediate states.

Fig. 4.13 for the explanation of the momentum and coordinate labeling). At the same time we impose no ordering on the transverse momenta of the quarks and the gluon. The kinematics is different from the DGLAP case (cf. Sec. 2.4.2): here the longitudinal momenta are ordered while in the DGLAP case the transverse momenta were ordered. In analogy with Eq. (2.68), we can write down the following expression for the $q\bar{q}G$ (one-gluon) contribution to the onium light cone wave function in the $A^+ = 0$ gauge at order g:

$$\begin{aligned}
&\Psi^{(1)}_{\sigma\sigma'}(\vec{k}_{1\perp}, \vec{k}_{2\perp}, z_1, z_2) \\
&\quad = \frac{g t^a \theta(k_2^+)}{k_2^- + k_1^- + (p-k_1-k_2)^- - p^-} \\
&\qquad \times \sum_{\sigma''=\pm 1} \left[\frac{\bar{u}_\sigma(k_1)\gamma \cdot \epsilon^*_\lambda(k_2) u_{\sigma''}(k_1+k_2)}{k_1^+ + k_2^+} \Psi^{(0)}_{\sigma''\sigma'}(\vec{k}_{1\perp} + \vec{k}_{2\perp}, z_1 + z_2) \right. \\
&\qquad\qquad \left. - \frac{\bar{v}_{\sigma''}(p-k_1)\gamma \cdot \epsilon^*_\lambda(k_2) v_{\sigma'}(p-k_1-k_2)}{p^+ - k_1^+} \Psi^{(0)}_{\sigma\sigma''}(\vec{k}_{1\perp}, z_1) \right].
\end{aligned} \tag{4.56}$$

Here a is the gluon color index, σ, σ', and σ'' are the quark and antiquark polarizations, and λ is the gluon polarization $z_2 = k_2^+/p^+$ and $z_1 = k_1^+/p^+$.

To simplify Eq. (4.56) we first remember that we have assumed that $k_2^+ \ll k_1^+, p^+ - k_1^+$ (that is $z_2 \ll z_1, 1 - z_1$) and that all the transverse momenta are comparable. In this kinematics the light cone energy of the gluon, $k_2^- = k_{2\perp}^2/k_2^+$, dominates the energy denominator, just as in the DGLAP case (cf. Eq. (2.69)), only now this is due to longitudinal momentum ordering. We can write

$$\frac{1}{k_2^- + k_1^- + (p-k_1-k_2)^- - p^-} \approx \frac{1}{k_2^-} = \frac{k_2^+}{k_{2\perp}^2}. \tag{4.57}$$

To evaluate the Dirac matrix elements in Eq. (4.56) we use Table A.1 along with Eq. (A.2), again keeping in mind that $k_2^+ \ll k_1^+, p^+ - k_1^+$. For instance, the contents of the first matrix

P1: SFK Trim: 247mm × 174mm Top: 13.707mm Gutter: 18.98mm
CUUK1947-04 CUUK1947/Kovchegov 978 0 521 11257 4 March 23, 2012 20:28

element in the square brackets of Eq. (4.56) simplify to

$$\bar{u}_\sigma(k_1)\gamma\cdot\epsilon^*_\lambda(k_2)u_{\sigma''}(k_1+k_2)\approx\frac{1}{2}\bar{u}_\sigma(k_1)\gamma^+u_{\sigma''}(k_1+k_2)\epsilon^-_\lambda(k_2)^*$$
$$=2\delta_{\sigma\sigma''}\sqrt{k_1^+(k_1^++k_2^+)}\,\frac{\vec{\epsilon}^{\,\lambda*}_\perp\cdot\vec{k}_{2\perp}}{k_2^+}\approx 2\delta_{\sigma\sigma''}k_1^+\frac{\vec{\epsilon}^{\,\lambda*}_\perp\cdot\vec{k}_{2\perp}}{k_2^+}. \tag{4.58}$$

Performing a similar approximation for the second matrix element in Eq. (4.56) and inserting the result along with Eqs. (4.57) and (4.58) back into Eq. (4.56) yields

$$\Psi^{(1)}_{\sigma\sigma'}(\vec{k}_{1\perp},\vec{k}_{2\perp},z_1,z_2)$$
$$\approx 2gt^a\theta(z_2)\frac{\vec{\epsilon}^{\,\lambda*}_\perp\cdot\vec{k}_{2\perp}}{k_{2\perp}^2}\left[\Psi^{(0)}_{\sigma\sigma'}(\vec{k}_{1\perp}+\vec{k}_{2\perp},z_1)-\Psi^{(0)}_{\sigma\sigma'}(\vec{k}_{1\perp},z_1)\right], \tag{4.59}$$

where we have also neglected z_2 in comparison with z_1 in the argument of one wave function.

In the transverse coordinate space representation, Eq. (4.59) has the form

$$\Psi^{(1)}_{\sigma\sigma'}(\vec{x}_{10},\vec{x}_{20},z_1,z_2)=\int\frac{d^2k_{1\perp}d^2k_{2\perp}}{(2\pi)^4}e^{i\vec{k}_{1\perp}\cdot\vec{x}_{10}+i\vec{k}_{2\perp}\cdot\vec{x}_{20}}\Psi^{(1)}_{\sigma\sigma'}(\vec{k}_{1\perp},\vec{k}_{2\perp},z_1,z_2)$$
$$=i\frac{gt^a}{\pi}\Psi^{(0)}_{\sigma\sigma'}(\vec{x}_{10},z_1)\,\vec{\epsilon}^{\,\lambda*}_\perp\cdot\left(\frac{\vec{x}_{21}}{x_{21}^2}-\frac{\vec{x}_{20}}{x_{20}^2}\right), \tag{4.60}$$

where $\vec{x}_{20}=\vec{x}_{2\perp}-\vec{x}_{0\perp}$, $\vec{x}_{21}=\vec{x}_{2\perp}-\vec{x}_{1\perp}$, and $x_{ij}=|\vec{x}_{ij}|$ as defined after Eq. (1.87). The gluon has transverse coordinate $\vec{x}_{2\perp}$, as illustrated in Fig. 4.13. We have used Eq. (A.10) to obtain Eq. (4.60) from Eq. (4.59).

Squaring the coordinate-space one-gluon wave function from Eq. (4.60) and summing over the quark and gluon polarizations and colors yields

$$\sum_{\sigma,\sigma',\lambda,a}\left|\Psi^{(1)}_{\sigma\sigma'}\right|^2=\frac{4\alpha_s C_F}{\pi}\frac{x_{10}^2}{x_{20}^2x_{21}^2}\sum_{\sigma,\sigma'}\left|\Psi^{(0)}_{\sigma\sigma'}\right|^2. \tag{4.61}$$

To calculate the probability of finding one extra gluon in the onium wave function we have to integrate Eq. (4.61) over the gluon's phase space, which, in the $z_2\ll z_1$, $1-z_1\ll 1$ approximation, is (cf. Eq. (4.23))[4]

$$\int_{z_0}^{\min\{z_1,1-z_1\}}\frac{dz_2}{z_2}\int\frac{d^2x_2}{4\pi}, \tag{4.62}$$

where z_0 is some lower cutoff on the z_2-integral, imposed to make the integration finite; the exact value of z_0 depends on the physical process corresponding to the wave function we are constructing. The order-α_s contribution to the probability of finding one gluon inthe

[4] One may ask why, if our calculation is valid for $z_2\ll z_1$, $1-z_1$, we can extend the z_2-integral all the way up to z_1 or $1-z_1$. While indeed our approximation breaks down for z_2 close to z_1 or $1-z_1$, putting z_1 or $1-z_1$ as the upper integration limit gives the correct leading-logarithmic contribution.

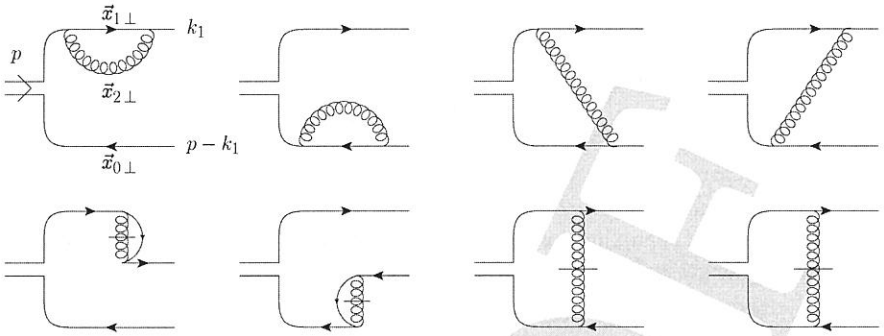

Fig. 4.14. Virtual contribution to small-x evolution in the onium wave function. The quark transverse coordinates in the onium are not changed by the corrections.

onium wave function is then (Mueller 1994)

$$\int\limits_{z_0}^{\min\{z_1,1-z_1\}} \frac{dz_2}{z_2} \int \frac{d^2x_2}{4\pi} \sum_{\sigma,\sigma',\lambda,a} \left|\Psi^{(1)}_{\sigma\sigma'}\right|^2 = \int\limits_{z_0}^{\min\{z_1,1-z_1\}} \frac{dz_2}{z_2} \int d^2x_2 \frac{\alpha_s C_F}{\pi^2} \frac{x_{10}^2}{x_{20}^2 x_{21}^2} \sum_{\sigma,\sigma'} \left|\Psi^{(0)}_{\sigma\sigma'}\right|^2 . \tag{4.63}$$

Note that the modified wave function in Eq. (4.63) contains a power of α_s and a logarithmic integral over z_2, which would give us finally $\ln 1/x$. We see that the modification we have calculated brings in a factor $\alpha_s \ln 1/x$. Another feature of Eq. (4.63) is that the $\vec{x}_{2\perp}$-integral in it contains UV divergences at $x_{20} \approx 0$ and $x_{21} \approx 0$. For now we will regulate these divergences by a UV cutoff ρ, such that $x_{20}, x_{21} > \rho$: in the end no physical quantity depends on the value of this cutoff.

Before we proceed let us point out that, as for the Glauber–Gribov–Mueller model (see e.g. Eq. (4.41)), the expression (4.63) completely factorizes transverse coordinate space into the square of the "bare" onium wave function times the probability of emission of the extra gluon. The emission of an extra gluon does not change the coordinates of the initial quark and the antiquark, yet again illustrating our above argument about the convenience of the transverse coordinate representation. This property also gives Eq. (4.61) a very simple physical meaning, resulting from the probabilistic interpretation of the light cone wave functions: the contribution to the onium wave function due to the emission of an extra gluon is equal to the product of the probability of finding a dipole with size x_{10} inside the onium ($\sim |\Psi^{(0)}_{\sigma\sigma'}|^2$) multiplied by the probability that the dipole emits a gluon at $\vec{x}_{2\perp}$.

The one-gluon corrections to the dipole wave function need not be limited to the "real" gluon shown in Fig. 4.13; they should also include virtual corrections, where the gluon is both emitted and absorbed in the onium wave function, again like in the DGLAP case in Sec. 2.4.2. The virtual diagrams giving the LLA contributions are shown in Fig. 4.14, where, in accordance with the LCPT rules introduced in Sec. 1.3, the crossed lines denote instantaneous terms. From the sheer number of graphs in Fig. 4.14 one can see that direct calculation of all the virtual corrections can be a daunting task (see Chen and Mueller